Synthesis and Multifaceted Exploration of 4-Phenylpiperidin-4-ol Substituted Pyrazole: Photophysical Insights with Biological Activity

Ghaferah H. Al-Hazmi[1], Vidyagayatri Marrakkur[2], Lohit Naik[3], Moamen S. Refat[4*]

[1]Department of Chemistry, College of Science, Princess Nourah bint Abdulrahman University, P.O. Box 84428, Riyadh 11671, Saudi Arabia
[2]Department of Chemistry, NMKRV College for Women, Bengaluru-560006, India
[3]Department of Physics and Electronics, CHRIST (Deemed to be University), Bengaluru-560029, India
[4]Department of Chemistry, College of Science, Taif University, P.O. Box 11099, Taif 21944, Saudi Arabia
Corresponding author: e-mail: msrefat@yahoo.com

In this study, we successfully synthesized a pyrazole derivative, specifically 4-phenylpiperidin-4-ol substituted pyrazole (CHP), through the reaction of Grignard reagents in combination with pyrazole. This newly synthesized molecule was subjected to a comprehensive evaluation for both its photophysical and biological applications. Notably, CHP exhibited promising *invitro* antifungal and antibacterial activities, primarily attributed to the presence of the 4-phenylpiperidin-4-ol moiety and resulting component contributed to an enhanced absorption rate of lipids, thereby improving the pharmacological activity of CHP. This correlation between structure and function was further supported by the outcomes of structure-activity relationship studies. Additionally, we conducted *in silico* studies to examine the molecular interactions of the synthesized molecule with key proteins, including DNA Gyrase, Lanosterol 14 α-demethylase, and KEAP1-NRF2. The results unveiled robust binding interactions at specific sites within these proteins, indicating potential therapeutic relevance. Furthermore, the photophysical properties of the synthesized compounds were thoroughly investigated using the *ab-initio* technique. This involved the determination of ground state optimization and HOMO-LUMO energy levels, all calculated with the DFT-B3LYP-6-31G(d) basis set. The assessment of the theoretically estimated HOMO-LUMO value provided insights into the global chemical reactivity descriptors, revealing that the synthesized molecule boasts a highly electronegative and electrophilic index. Taken together, our findings suggest that pyrazole derivatives with 4-phenylpiperidin-4-ol substitutions exhibit promising applications in both photophysical and biological contexts.

Keywords: Pyrazolones, *in-vitro* and *in-silico* biological activity, HOMO-LUMO.

INTRODUCTION

In the realm of applied organic chemistry, a pivotal and distinctive focus lies in nitrogen-based heterocyclic chemistry. Over the past two decades, substantial research efforts have been dedicated to pioneering compounds and composites within this domain. The allure of these compounds stems from their multifaceted applications in chemical sciences and their pivotal role in diverse organic synthesis methodologies[1].

Naturally occurring N-heterocyclic compounds boast physiological and pharmacological significance, serving as vital building blocks for biologically consequential substances. From vitamins and nucleic acids to medications, antibiotics, dyes, and agrochemicals, these molecules play pivotal roles[2]. Notably, N-heterocyclic compounds, such as purines and pyrimidines, constitute the base pairs of DNA and RNA, exemplified by guanine, cytosine, adenine, and thymine. This has not escaped the attention of the rapidly evolving pharmaceutical sector, organic chemistry, and medicinal chemistry fields, which recognize the distinctive properties and applications of nitrogen-containing heterocyclic compounds[3].

Moreover, nitrogen heterocycles, endowed with electron-rich properties, exhibit a remarkable capacity for forming various weak interactions and facile absorption or donation of protons. These encompass hydrogen bonding, dipole-dipole interactions, hydrophobic effects, Vander Waals forces, and π-stacking interactions, all gaining prominence in medicinal chemistry. The heightened solubility of nitrogen molecules enhances their interaction with enzymes and receptors in biological targets, showcasing their affinity. The diverse structural characteristics of their derivatives further amplify their utility, showcasing a spectrum of bioactivities.

A cursory exploration of FDA databases underscores the structural significance of nitrogen-based heterocycles in drug design and pharmaceutical engineering. In approximately 75% of cases, distinct small-molecule medicines contain nitrogen heterocycles. Recent comprehensive insights into the structural diversity, substitution trends, and prevalence of nitrogen heterocycles in FDA-approved medications, compiled by Vitaku and colleagues, underscore their pivotal role[4]. Owing to the nitrogen atom's predisposition to facilely establish hydrogen bonds with biological targets, these N-heterocyclic frameworks are intricately tied to therapeutic applications, forming the bedrock for numerous potential drug candidates[5]. The pyrimidine structure, integral to nucleic acids like DNA and RNA, imparts various therapeutic uses in medicinal chemistry[6]. Notably, a plethora of heterocyclic nitrogen-containing compounds exhibit diverse pharmacological properties, spanning anticancer, anti-HIV, antimalarial, anti-tubercular, antibacterial, antidiabetic and optoelectronic application[7–10].

The current undertaking aims at the synthesis of a 4-phenylpiperidin-4-ol substituted pyrazole derivative (CHP) and the assessment of its biological and photophysical properties through a combination of experimental and theoretical techniques.

Materials and methods

Commercial samples of high purity were utilized as received for the reagents (Fischer, Merck, and Sigma

Aldrich). An RB flask that had been oven-dried was used for the reactions. Alumina silica gel 60F254 (Fischer) underwent TLC after being detected by iodine vapors and UV light (254 nm). Uncorrected open capillaries on a Buchi apparatus were used to determine the melting points. Using KBr pellets, the IR spectra were captured on a Nicolet-Impact-410 FT-IR spectrometer. Using TMS as an internal standard and a Bruker AC-400F, 400MHz, spectrometer, the resonance frequencies for the ^{1}H-NMR and ^{13}C-NMR spectra were 400 MHz and 100 MHz, respectively. Agilent 1200 series equipment was used to conduct LCMS analyses. The Heraus CHN fast analyzer was used to do the elemental analysis. All of the compounds produced C, H, and N analyses that were within 0.4% of the predicted values.

Synthesis of 4-phenylpiperidin-4-ol substituted pyrazole derivative (CHP)

The synthesis of compound (3) commenced with the amalgamation of 1 mmol of β-diketoester and 4-fluorophenyl hydrazine in a solution comprising 100 ml of ethanol and 10 ml of acetic acid. The resultant mixture underwent overnight reflux, and post-ethanol concentration removal, neutralization with Na_2CO_3 ensued. The precipitated solid was filtered, dried, and subject to further purification via recrystallization in ethanol. Following this, pyrazole carboxylic acid ethyl ester (3), derived from 1 mmol of the compound, was dissolved in 50 ml of tetrahydrofuran (THF). To this solution, 15 ml of methanol, 20 ml of water, and 1.2 mmol of lithium hydroxide were added, initiating an overnight stirring process. After the reaction, solvent concentration removed volatile constituents, leaving behind a residue that dissolved in a solution comprising 50 ml of water and 100 ml of ethyl acetate. The resultant solution underwent acidification to achieve a pH of approximately 5 using 1N HCl and was then subjected to extraction with 100 ml of ethyl acetate, repeated twice. The amalgamated organic layers were washed with 50 ml of water and a brine solution (20 ml), dried with Na_2SO_4, and evaporated to yield Compound (4).

In the preparation of Compound (5), 1 mmol of Compound (4) dissolved in 20 ml of dichloromethane (DCM) was subjected to the addition of 1.5 mmol of oxalyl chloride at 0°C. After a 5-minute interval, a catalytic amount of dimethylformamide (DMF) in the form of 3 drops was introduced, and the mixture was stirred at room temperature. Following the completion of the reaction, excess oxalyl chloride was eliminated under nitrogen, resulting in the formation of pure acid chloride. This acid chloride, dissolved in fresh DCM (25 ml), had 2 mmol of triethylamine added at 0 ºC, followed by the introduction of 1.1 mmol of 4-piperidone, also at 0 ºC. Upon completion of the reaction, the mixture was diluted with 50 ml of water and subjected to DCM extraction twice (2×100 ml). The amalgamated organic layer underwent washing with 50 ml of water and a brine solution (20 ml), drying with Na_2SO_4, and evaporation to dryness. The crude products were subsequently purified by washing with diethyl ether.

Ultimately, for the preparation of Compound (6), 1 mmol of Compound (5) was taken in THF (20 ml), and 1.5 mmol of Grignard reagent was introduced at 0 ºC. Once the reaction reached completion, the mixture was allowed to attain room temperature, monitored by TLC. The reaction mixture underwent quenching with saturated ammonium chloride and extraction with ethyl acetate twice (2×100 ml). The combined organic layer underwent washing with 50 ml of water and a brine solution (20 ml), drying over Na_2SO_4, and evaporation to dryness. The crude products were purified by column chromatography employing 230–400 silica gel.

Structural characterization of (5-(4-chlorophenyl)-1-(4-fluorophenyl)-1H-pyrazol-3-yl)(4-hydroxy-4-phenylpiperidin-1-yl)methanone (CHP)

White solid, mp 86.5 ºC; % Yield: 68; ^{1}H NMR (300 MHz, CDCl$_3$): δ = 7.49(d, 2H, ArH), 7.38(m, 6H, ArH), 7.36(m, 1H, ArH), 7.27(m, 2H, ArH), 7.09(m, 2H, ArH), 6.91(s, 1H, pyrazole CH), 4.76(m, 2H, -CH$_2$), 3.71(m, 1H, -CH), 3.37(m, 1H, -CH), 2.16(m, 2H, -CH$_2$), 1.87(m, 2H, -CH$_2$); MS calcd. for C$_{27}$H$_{23}$ClFN$_3$O$_2$: 475.94, Found: 476.2(M +); IR (ν cm^{-1}): 3360(O-H), 2922(C-H), 2193(C-H), 1600(C=O); Elem. Anal. cald (found): C: 68.14(68.12), H: 4.87(4.85), N: 8.83(8.85).
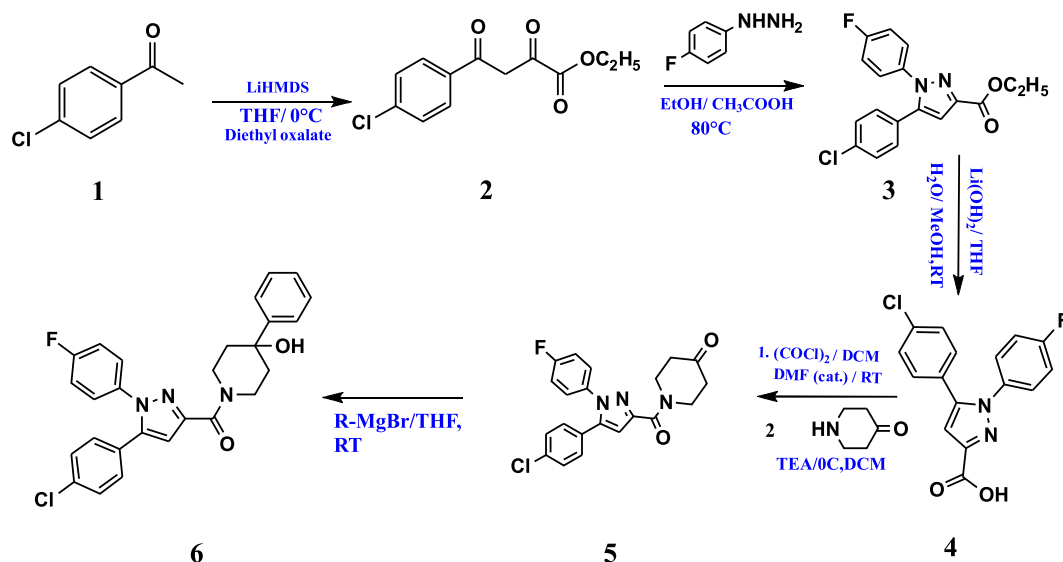
Scheme 1. Synthesis of 4-phenylpiperidin-4-ol substituted pyrazole derivative

RESULTS AND DISCUSSION

Computational photophysical studies

Molecular orbitals, with their associated properties and energy levels, stand as invaluable tools for physicists and chemists alike. These orbitals, particularly the frontier electron density, play a crucial role in predicting reactive positions within π-electron systems and in understanding various reactions within conjugated systems[11–13]. Furthermore, the eigenvalues of the highest occupied molecular orbital (HOMO) and the lowest unoccupied molecular orbital (LUMO), along with the energy gap between them, offer profound insights into the chemical reactivity of a molecule. Recently, the energy gap between the HOMO and LUMO has found application in illustrating the bioactivity arising from intramolecular charge transfer (ICT)[14–15].

The optimization of the ground state for the recently synthesized 4-phenylpiperidin-4-ol substituted pyrazole derivative (CHP) was conducted using the DFT-B3LYP/6-31G (d) basis set within the Gaussian-09W software. The choice of basis set in computational chemistry profoundly influences the accuracy and efficiency of calculations. Among these sets, the DFT-B3LYP/6-31G(d) basis set stands out for its balanced performance in capturing molecular properties. Specifically tailored for organic molecules, the 6-31G(d) basis set incorporates diffuse functions, denoted by the (d), which enhance its ability to describe electronic correlation effects in molecules with polar bonds or lone pairs. This inclusion is particularly advantageous when studying systems involving heavy atoms like oxygen and halogens. Coupled with the B3LYP functional, this basis set strikes a delicate balance between accuracy and computational cost, making it widely applicable in density functional theory calculations. While larger basis sets may offer greater precision, they often come at a significantly higher computational expense. The 6-31G(d) basis set, therefore, serves as a pragmatic choice, providing satisfactory accuracy while maintaining computational efficiency, thus catering to diverse research needs across organic chemistry and beyond. The optimized molecular geometry and the HOMO-LUMO energy plot of the CHP molecule are presented in Figs. 1–2. Examination of the HOMO-LUMO plot reveals that the π-orbital of the HOMO-LUMO electron cloud predominantly distributes over 5-(4-chlorophenyl)-1-(4-fluorophenyl)-1H-pyrazole-3-carbaldehyde.

To gain insight into the chemical reactivity and stability of CHP molecules, global reactivity parameters[16], were estimated using the following equations

$$\eta = \frac{(IP - EA)}{2} \tag{1}$$

$$\chi = \frac{(IP + EA)}{2} \tag{2}$$

$$\mu = -\chi \tag{3}$$

$$S = \frac{1}{2\eta} \tag{4}$$

$$\omega = \frac{\mu^2}{2\eta} \tag{5}$$

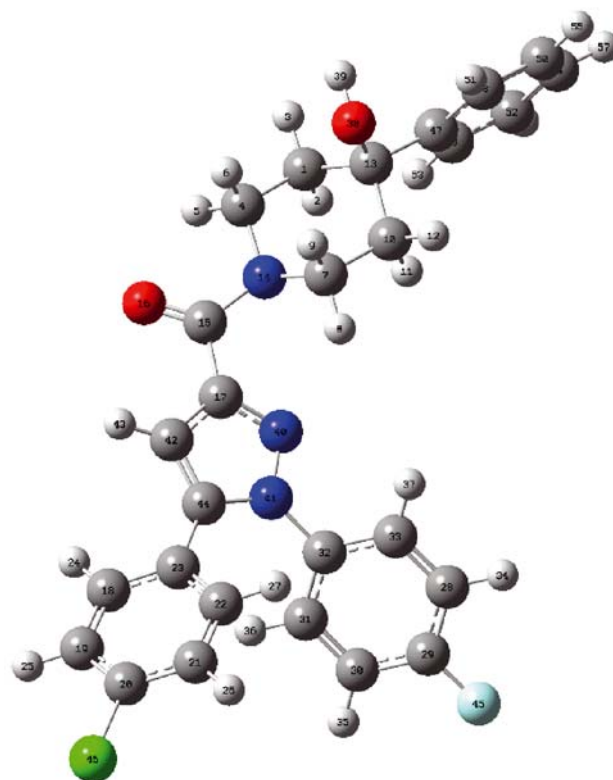Chemical hardness (η = 2.307 eV), electronegativity (χ = 3.824 eV), chemical potential (μ = –3.824 eV),

Figure 1. Optimised molecular geometry with atomic labels of the CHP molecule

E_{LUMO} = -1.517 eV

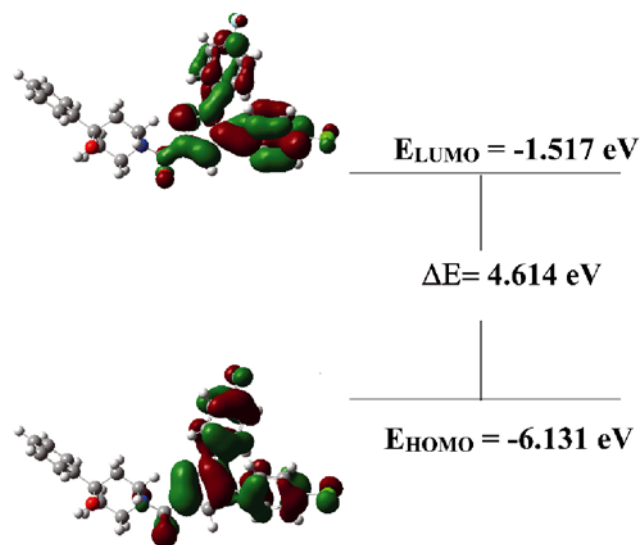ΔE = 4.614 eV

E_{HOMO} = -6.131 eV

Figure 2. 3D plots of HOMO-LUMO with energy levels for CHP molecule

chemical softness (S = 0.217 eV) and electrophilicity index (ω = 3.169 eV) were calculated from E_{HOMO} and E_{LUMO} values[17], where, ionization potential, $IP = -E_{HOMO}$ = 5.428 eV and electron affinity, EA = $-E_{LUMO}$ = 1.326 eV. While a wider HOMO–LUMO gap is connected with stability and hardness, a lesser HOMO–LUMO gap signifies a more reactive soft molecule that is highly polarizable.

The energy levels of molecular orbitals play a pivotal role in understanding the reactivity and stability of compounds, with a focus on the highest occupied molecular orbital (HOMO) and the lowest unoccupied molecular orbital (LUMO). The LUMO, acting as an electron acceptor during molecular interactions, correlates with

the electron affinity (EA = $-E_{LUMO}$). Conversely, the HOMO, representing electron donors, is associated with the ionization potential (IP = $-E_{HOMO}$). A substantial HOMO-LUMO energy gap indicates high kinetic stability and low chemical reactivity, making it energetically unfavorable to add electrons to the high-lying LUMO or remove electrons from the low-lying HOMO. The compound FHM, formed through the non-planar attachment of 4-hydroxy-4-phenylpiperidine-1-carbaldehyde to pyrazole, exhibits a large energy gap, rendering it hard and more chemically stable according to the GCRD measure. This non-planar attachment induces the greatest energy gap, making the five-membered ring more reactive.

Minor perturbations significantly influence the deformation of the molecular electron cloud, showcasing the underlying resistance contributing to hardness in chemical processes. In contrast to larger, more polarizable soft molecules, hard molecules are relatively smaller with reduced polarizability. The hardness of a molecule is crucial in conveying stability and intermolecular reactivity, with electrophilicity phenomena closely tied to an electrophile's ability to acquire additional electrical charge.

The electrophilicity index, derived from HOMO-LUMO energy values, serves as a key quantum chemical descriptor for assessing reactivity and site selectivity, especially in terms of toxicity. A lower value of ω denotes a strong nucleophile, while higher ω values signify potent electrophiles. Organic molecules with electrophilicity scales (ω) exceeding 1.5 eV are considered robust electrophiles, those ranging between 0.8 eV and 1.5 eV are deemed moderate electrophiles, and those below 0.8 eV are classified as weaker electrophiles.

Our research findings indicate that the CHP molecules possess strong electrophilic characteristics, evident in their elevated ω values. The chemical potential (μ), reflecting the propensity of electrons to exit a stable system, reveals that FHM molecules, with negative chemical potentials, do not spontaneously disintegrate. The HOMO-LUMO gap at an energy level of 4.614 eV indicates low polarizability, demonstrating resistance to electron cloud deformation under moderate disturbances within the chemical system[18–19].

In vitro antimicrobial, antifungal, and antioxidant activity

The newly synthesized compound CHP was the subject of antimicrobial investigations, yielding remarkable antibacterial efficacy against *S. aureus*, *B. subtilis*, *S. typhi*, and *E. coli*, as detailed in Table 1. Moreover, the CHP molecule demonstrated strong antifungal activity against *A. niger* and *C. albicans*, with specific data provided in Table 1. The enhanced activity of the compound can be attributed to the presence of biologically active components, including the pyrazole moiety and the 4,4-dimethylpiperidine ring and its bears similarities

to hydrogen in terms of steric requirements at enzyme receptor sites. The inclusion of 4,4-dimethylpiperidine contributes to an accelerated absorption rate due to its heightened lipid solubility, an attribute that significantly augments the molecules' pharmacological potential[20]. The pronounced lipophilic nature of the bromobenzene group plays a pivotal role in enhancing pharmacological activity. Furthermore, we evaluated the antioxidant properties of CHP molecules and found them to possess exceptional radical scavenging capabilities at the tested concentration of 15μM, as evidenced in Table 2, in comparison to the standard reference, edaravone. The observed variations in DPPH scavenging capacity can be linked to the impact of diverse substitutions at positions 1, 2, 3 and 5 within the synthesized compounds. These antioxidant activity results align with those seen in previous research findings[21].

Table 2. DPPH scavenging assay of CHP

Compounds Concentration (15ěg/mL)	CHP	Standard (edaravone)
% DPPH scavenging	53.78	73.16

Molecular docking studies

Conducting molecular docking simulations, we employed the AutoDock VINA software integrated into the PyRx 0.8 virtual screening tool[22] to evaluate binding affinity. In silico docking studies were carried out to assess the molecular interactions of the CHP compound with specific protein targets, namely DNA Gyrase (PDB: 2XCT) as an antibacterial target, Lanosterol 14 alpha demethylase or CYP51 (PDB: 4WMZ) as an antifungal target, and KEAP1/NRF2 (PDB: 6QME) as an antioxidant target, all with a co-crystallized ligand (J6Q).

For optimal configurations in subsequent docking studies, meticulous preparation of protein structures was performed using the UCSF Chimera Dock Prep module. This process involved removing water molecules and other ligands, adding any missing atoms and residues, energy minimization, and assigning charges and polar hydrogens. The resulting structures were then converted into the pdbqt format. Simultaneously, ligands' 2D structures were sketched using ChemDraw software, followed by structural optimization through energy minimization using MMFF94 force field parameters and a conjugate gradient algorithm. This ligand optimization was facilitated by the Open Babel module of PyRx, converting the ligands into an AutoDock-compatible pdbqt format for subsequent docking exploration.

To facilitate docking studies, an AutoDock grid box was meticulously positioned around the binding site where the co-crystallized ligand was located. Subsequent analysis and visualization of docking results, binding poses, and molecular interactions were carried out using a suite of tools, including BIOVIA Discovery Studio 2021, Molegro

Table 1. Antimicrobial and antifungal activity of the CHP

Compound	*S. aureus*	*B. subtilis*	*S. typhi*	*E. coli*	*A. niger*	*C. albicans*
CHP	27	31	28	28	25	26
Standard[a]	24	23	23	25	25	24
Control[b] DMSO	0	0	0	0	0	0

Note: [a]Standard drug used: Bacteria (Ciprofloxacin), Fungal (Fluconazole) were in 40 μg in 100μL, and R: Resistance
[b]Control: DMSO (Dimethyl sulphoxide)

Molecular Viewer, and Chimera X[23-25]. Comparisons of binding energies and molecular interaction profiles of the compounds were made with co-crystallized inhibitory ligands in DNA Gyrase, Lanosterol 14 alpha-demethylase, and KEAP1/NRF2 proteins. A summary of these values is presented in Table 3, while Table 4 details the precise binding site positions of FHM with different proteins.

With a binding energy of –3.4 Kcal/mol, the substance CHP positioned itself at the DNA-protein interface. In this binding orientation, the hydroxy group on piperidinyl and the fluorine group on the phenyl group connected to the pyrazole ring, respectively, allowed CHP to create two H-bond interactions with the GLU477 and ASP437 active site residues. ARG458 had interactions with amide-π stacks and π− alkyls with pyrazole and fluorine substituted phenyl rings, respectively, whereas ASP437 contributed via the -OH group. With a phenyl ring replaced with a chlorine group, LYS60 exhibited π-donor hydrogen bond interactions, and nearby amino acids displayed Vander Waals interactions. A visual representation of the molecular interactions, binding site, and binding pose of CHP is given in Fig. 3.
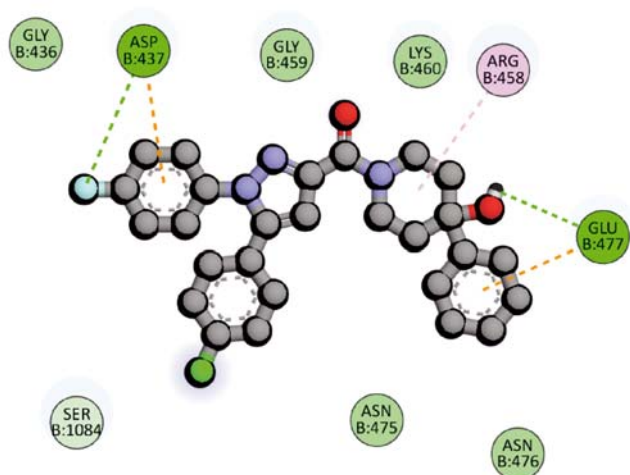

Figure 3. 2D representation of the binding poses of CHP in the active site of Staphylococcus aureus DNA gyrase

CHP demonstrated a superior binding energy of –9.3 Kcal/mol when interacting with the antifungal target Lanosterol 14α demethylase compared to Fluconazole, which exhibited a binding energy of –7.1 Kcal/mol. CHP engaged in a hydrogen bond interaction with GLN150, TYR126 similar to Fluconazole, utilizing the oxygen of its ester group. It also formed π-σ interactions with LEU147, TYR140 and VAL138 residues. Furthermore, PHE236 established π-π T-shaped interactions with the pyrazole ring, while the HEM moiety of the cytochrome and ILE139, LEU147, LYS15, and VAL311 residues participated in alkyl interactions with CHP 's long aliphatic side chain. Additionally, CHP exhibited Van der Waals interactions with surrounding amino acid residues within the binding site. To visualize these molecular interactions, the binding site, and the binding pose of CHP, please refer to Fig. 4.
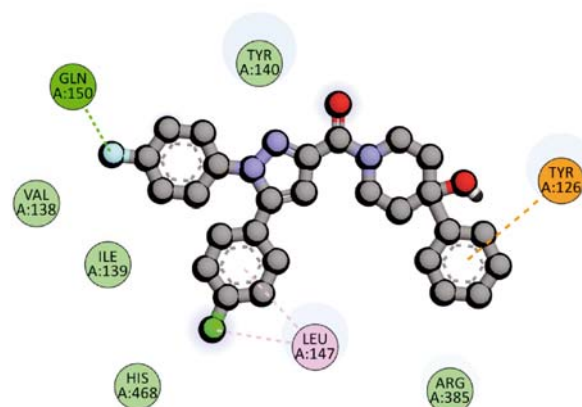

Figure 4. 2D representation of the binding poses of CHP and in the active site of S. cerevisiae Lanosterol 14α demethylase

On the other hand, Fluconazole displayed a somewhat lower binding energy of –7.8 Kcal/mol compared to CHP. It formed a hydrogen bond with TYR140 and was further stabilized through various interactions. These interactions included π-σ interactions with LEU380, π-π stacked, and π-π T-shaped interactions with TYR126 and PHE236 residues, primarily facilitated by the triazole rings. The HAEM moiety also engaged in a hydrophobic interaction with the difluoro-substituted aromatic ring. In addition, ILE139, HIS468 and ARG385 residues contributed pi-alkyl interactions with the triazole and halogen-substituted ring, while GLY314 established halogen interactions with the fluorine groups. For a clearer understanding of these interactions, the binding site, and the binding configuration of CHP and Fluconazole, please refer to Fig. 4.

Table 3. Binding energy (Kcal/mol) summary of CHP compound with the three target proteins

Compounds	DNA Gyrase	Lanosterol 14α demethylase	KEAP1/NRF2
CHP	−3.4	−8.3	−7.2
Ciprofloxacin	−4.6	−	−
Fluconazole	−	−7.8	−
J6Q	−	−	−8.5
Edaravone	−	−	−6.1

Table 4. Molecular interaction summary of CHP compound with different target proteins

Target Protein	Binding Energy (K.cal/mol)	Interacting Amino acids	Nature of interaction
DNA Gyrase	−3.4	GLU477, ASP437, ARG458, LYS460, GLY459, GLY436, ASN475, ASN476	H-bond, Hydrophobic (Alkyl, π–Alkyl), Vander Waals
Lanosterol 14 alpha demethylase	−8.3	GLN150, TYR126, LEU147, TYR140, VAL138, ILE139, HIS468, ARG385	H-bond, Hydrophobic (π–Alkyl, Alkyl, π–σ, π− π–T-shaped), Vander Waals
KEAP1-NRF2	−7.2	SER555, GLN530, SER602, TYR525, ALA556, TYR334, GLN528, GLY574, ARG483, ASN382, SER363, GLY603, PHE577	H-bond, Hydrophobic (Alkyl, π–Alkyl, π–σ), Vander Waals

The compound CHP exhibited structural similarities to edaravone, a neuroprotective agent known for its antioxidant mechanism. The NRF2-KEAP1 pathway serves as a pivotal regulator in this mechanism, and literature reports have highlighted edaravone's activity through NRF2. As a result, edaravone was selected as the antioxidant target for in silico analysis of molecular interactions. In this analysis, CHP displayed a superior binding energy of -7.2 Kcal/mol compared to edaravone (–6.1 Kcal/mol) but fell slightly short of J6Q (–8.5 Kcal/mol). Notably, CHP established a hydrogen bond interaction with SER602 via the -C=O of its aliphatic ester side chain. Additionally, SER555, ARG483, ASN382, and SER363 engaged in π-σ interactions, with these residues, along with PHE577, also participating in alkyl interactions with the elongated aliphatic ester side chain. ALA556 exhibited π-alkyl interactions with both the aromatic and pyrazole rings. ARG415 contributed to both alkyl and π-alkyl interactions with the pyrazole ring, alongside other active residues in close proximity. ARG483, ASN382, SER363, In contrast, edaravone displayed a single hydrogen bond interaction with ALA556 and a pi-alkyl interaction with ARG415. J6Q, on the other hand, formed two hydrogen bonds with SER602 and SER508 active site residues, facilitated by the nitrogen of the benzotriazole ring and the sidechain propanoic acid, respectively. Notably, both CHP and J6Q shared a common hydrogen bond interaction with SER602. Furthermore, interactions included pi-pi stacking between the chloro-substituted phenyl ring and TYR525, π-σ and π-alkyl interactions between ALA556 and the aromatic ring region of benzotriazole, as well as π-alkyl interactions between GLY603, PHE577 and the chlorine on the phenyl ring. CHP and J6Q compounds both interacted with critical active site residues like SER602, TYR525, TYR572, and ALA556. For a visual representation of these molecular interactions and the orientation of CHP in the protein's active site, please refer to Fig. 5. Overall, CHP demonstrated comparable and superior binding energy and interaction profiles compared to co-crystallized inhibitors in all three explored targets. The post-docking analysis suggests a strong in silico-in vitro correlation for the CHP compound, making it
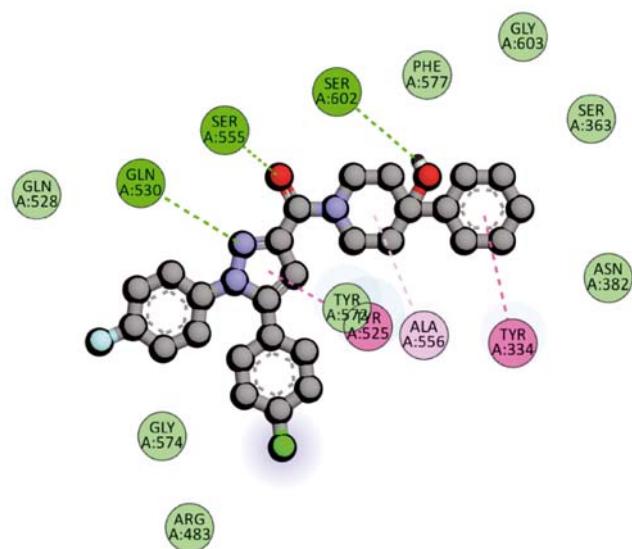
a potential candidate for antimicrobial and antioxidant applications. Similarly, the CHP compound warrants further investigation into its antioxidant mechanism via the Keap1-Nrf2 pathway, with the potential to develop as a promising novel compound[26-28].

CONCLUSIONS

In this study, we conducted the synthesis of 4-phenyl-piperidin-4-ol substituted pyrazole derivative derivatives with a high degree of functionalization, referred to as CHP. We thoroughly characterized the physicochemical properties of CHP using various analytical techniques, including ^{1}H-NMR, FT-IR, and LC-MS analysis. To gain insights into the photophysical properties of these compounds, we employed computational techniques. We utilized the DFT-B3LYP-6-31G(d) basis set to optimize the molecular geometry and generate important data such as HOMO-LUMO energy levels plot. Our analysis of these theoretical parameters indicated that CHP exhibits notable electrophilic characteristics, underscoring its reactivity, although it may possess relatively lower stability. Through our DFT computational investigations, we identified electron-deficient sites within the CHP molecule, which could be strategically employed in the development of pharmaceutical compounds for various biological applications. Moving beyond theoretical analysis, we evaluated the in-vitro antimicrobial, antifungal, and antioxidant activities of the CHP compound. Our results demonstrated the high potential of this molecule for biological applications. Moreover, we conducted in-silico molecular docking studies, which revealed that the synthesized CHP molecule exhibits superior interactions with target receptors such as ciprofloxacin, fluconazole, and edaravone, with binding energies falling in the range of –10.0 to –8.5 kcal/mol. This binding affinity exceeded that of the standard medicinal drug Rifampicin (–8.6 kcal/mol). These findings highlight the potential of the CHP molecule as an effective candidate in drug design, with the capacity to contribute to the regulation of pathogenic behavior. In summary, our results suggest that CHP holds promise for various biological applications, showcasing its potential as a valuable compound in the realm of drug development and the modulation of pathogen-related processes.

ACKNOWLEDGMENTS

LITERATURE CITED

1. Li, X., He, L., Chen, H., Wu, W. & Jiang, H. (2013). Copper-catalyzed aerobic C(sp2)–H functionalization for C–N bond formation: Synthesis of pyrazoles and indazoles. *J. Org. Chem*. 78, 3636–3646. DOI: 10.1021/jo400162d.

2. Eftekhari-Sis, B., Zirak, M. & Akbari, A. (2013). Aryl-glyoxals in synthesis of heterocyclic compounds. *Chem. Rev*. 113, 2958–3043. DOI: 10.1021/cr300176g.

3. Fang, W.Y., Ravindar, L., Rakesh, K.P., Manukumar, H.M., Shantharam, C.S., Alharbi, N.S. & Qin, H.L. (2019). Synthetic approaches and pharmaceutical applications of chloro-conta-

Figure 5. Representation of the binding poses of CHP molecule and in the active site of KEAP1-NRF2 protein

ining molecules for drug discovery: A critical review. *Eur. J. Med. Chem*. 173, 117–153. DOI: 10.1016/j.ejmech.2019.03.063.

4. Vitaku, E., Smith, D.T. & Njardarson, J.T. (2014). Analysis of the structural diversity, substitution patterns, and frequency of nitrogen heterocycles among U.S. FDA approved Pharmaceuticals. *J. Med. Chem*. 57, 10257–10274. DOI: 10.1021/jm501100b.

5. Gordon, E.M., Barrett, R.W., Dower, W.J., Fodor, S.P.A. & Gallop, M.A. (1994). Applications of combinatorial technologies to drug discovery, combinatorial organic synthesis, library screening strategies, and future directions. *J. Med. Chem*. 37, 1385–1401. DOI: 10.1021/jm00036a001.

6. Kaur, R., Chaudhary, S., Kumar, K., Gupta, M.K. & Rawal, R.K. (2017). Recent synthetic and medicinal perspectives of dihydropyrimidinones: A review. *Eur. J. Med. Chem*. 132, 108–134. DOI: 10.1016/j.ejmech.2017.03.025.

7. Chaudhari, K., Surana, S., Jain, P. & Patel, H.M. (2016). Mycobacterium tuberculosis (MTB) GyrB inhibitors: An attractive approach for developing novel drugs against TB. *Eur. J. Med. Chem*. 124, 160–185. DOI: 10.1016/j.ejmech.2016.08.034.

8. Akhtar, J., Khan, A.A., Ali, Z., Haider, R. & Yar, M.S. (2017). Structure-activity relationship (SAR) study and design strategies of nitrogen-containing heterocyclic moieties for their anticancer activities. *Eur. J. Med. Chem*. 125, 143–189. DOI: 10.1016/j.ejmech.2016.09.023.

9. Kaur, R., Dahiya, L. & Kumar, M. (2017). Fructose-1,6-bisphosphatase inhibitors: A new valid approach for management of type 2 diabetes mellitus. *Eur. J. Med. Chem*. 141, 473–505. DOI: 10.1016/j.ejmech.2017.09.029.

10. Alkathiri, A.A., Atta, A.A., Refat, M.S., Shakya, S., Hassanien, A.M., Algarni, S.A., Ahmed, E.M.A.; Alomariy, S.E., Alsawat, M. & Algethami, N. (2023). Impedance spectroscopy and DFT/TD-DFT studies of diyttrium trioxide for optoelectronic fields. *J. Rare Earths*, 41(4), 605–612. DOI: 10.1016/j.jre.2022.03.010.

11. Devasia, J., Chinnam, S., Khatana, K., Shakya, S., Joy, F., Rudrapal, M. & Nizam, A. (2023). Synthesis, DFT and In Silico Anti-COVID Evaluation of Novel Tetrazole Analogues. *Polycycl. Aromat. Compd*. 43(3), 1941–1956. DOI: 10.1080/10406638.2022.2036778.

12. Hussen, N.H., Hasan, A.H., Jamalis, J., Shakya, S., Chander, S., Kharkwal, H., Murugesan, S., Bastikar, V.A. & Gupta, P. P. (2022). Potential inhibitory activity of phytoconstituents against black fungus: In silico ADMET, molecular docking and MD simulation studies. *Computational Toxicology*, 24, 100247. DOI: 10.1016/j.comtox.2022.100247.

13. Lohit. N., Maridevarmath C.V., Khazi I.A.M. & Malimath G.H. (2019). Photophysical and computational studies on optoelectronically active thiophene substituted 1,3,4-oxadiazole derivatives, *J. Photochem. Photobio. A Chem*. 368, 200–209. DOI: 10.1016/j.jphotochem.2018.09.038.

14. Walki, S., Malimath, G.H., Mahadevan, K.M., Naik, S., Sutar, S. M., Savanur, H. & Naik, L. (2021). Synthesis, spectroscopic properties, and DFT correlative studies of 3, 3′-carbonyl biscoumarin derivatives. *J. Mol. Struct.* 1243, 130781. DOI: 10.1016/j.molstruc.2021.130781.

15. Prabhala, P., Sutar, S.M., Manjunatha, M.R., Pawashe, G.M., Gupta, V.K., Naik, L. & Kalkhambkar, R.G. (2022). Synthesis, in vitro and theoretical studies on newly synthesized deep blue emitting 4-(p-methylphenylsulfonyl-5-aryl/alkyl) oxazole analogues for biological and optoelectronic applications. *J. Mol. Liq.* 360, 119520. DOI: 10.1016/j.molliq.2022.119520.

16. Naik, L., Thippeswamy, M.S., Praveenkumar, V., Malimath, G.H., Ramesh, D., Sutar, S. & Bubbly, S.G. (2023). Solute-solvent interaction and DFT studies on bromonaph-

thofuran 1, 3, 4-oxadiazole fluorophores for optoelectronic applications. *J. Mol. Graph. Model*. 118, 108367. DOI: 10.1016/j.jmgm.2022.108367.

17. Parr, R.G. & Yang, W. (1989). *Density Functional Theory of Atoms and Molecules*, Oxford University Press, New York.

18. Alsanie, W.F., Alamri, A.S., Alyami, H., Alhomrani, M., Shakya, S., Habeeballah, H., Alkhatabi, H.A., Felimban, R.I. Alzahrani, A.S., Alhabeeb, A.A., Raafat, B.M. & Gaber, A. (2022). Increasing the Efficacy of Seproxetine as an Antidepressant Using Charge–Transfer Complexes. *Molecules*, 27(10), 3290. DOI: 10.3390/molecules27103290.

19. Islam, M., Khan, I.M., Shakya, S. & Alam, N. (2023). Design, synthesis, characterizing and DFT calculations of a binary CT complex co-crystal of bioactive moieties in different polar solvents to investigate its pharmacological activity. *J. Biomol. Struct. Dyn*. 41(20), 10813–10829. DOI: 10.1080/07391102.2022.2158937.

20. Domingo, L.R., Gutiérrez, M. & Pérez, P. (2016). Applications of the conceptual density functional theory indices to organic chemistry reactivity, *Molecules*, 21, 748. DOI: 10.3390/molecules21060748.

21. Reddy, G.M. & Camilo A. (2020). Biologically active dihydropyridines: an efficient green synthesis, antimicrobial properties, machine aided results and SARs, *Sust. Chem. Pharm*. 17, 100303. DOI: 10.1016/j.scp.2020.100303.

22. Fahim, A.M., Tolan, H.E. & El-Sayed, W.A. (2022). Synthesis of novel 1, 2, 3-triazole based Acridine and benzothiazole scaffold N-glycosides with anti-proliferative activity, docking studies, and comparative computational studies, *J. Mol. Struct*., 1251, 131941. DOI: 10.1016/j.molstruc.2021.131941.

23. Sargis, D. & Arthur, J.O. (2017). Small-molecule library screening by docking with PyRx, *Methods in molecular biology (Clifton, N.J.)*, 1263, 243–250.

24. Bax, B.D., Chan, P.F., Eggleston, D.S., Fosberry, A., Gentry, D.R., Gorrec, F., Giordano, I., Hann, M.M., Hennessy, A., Hibbs, M., Huang, J., Jones, E., Jones, J., Brown, K.K., Lewis, C.J., May, E.W., Saunders, M.R., Singh, O., Spitzfaden, C., Shen, C., Shillings, A., Theobald, A.F., Wohlkonig, A., Pearson, N.D. & Gwynn, M.N. (2010). Type IIA topoisomerase inhibition by a new class of antibacterial agents, *Nature*, 466, 935–940. DOI: 10.1038/nature09197.

25. Sagatova, A.A., Keniya, M.V., Wilson, R.K., Monk, B.C. & Tyndall, J.D. (2015). Structural Insights into Binding of the Antifungal Drug Fluconazole to Saccharomyces cerevisiae Lanosterol 14 alpha-Demethylase, Antimicrob. Agents Chemother. 59, 4982–4989. DOI: 10.1128/aac.00925-15.

26. Heightman, T.D., Callahan, J.F., Chiarparin, E., Coyle, J.E., Griffiths-Jones, C., Lakdawala, A.S., McMenamin, R., Mortenson, P.N., Norton, D., Peakman, T.M., Rich, S.J., Richardson, C., Rumsey, W.L., Sanchez, Y., Saxty, G., Willems, H.M.G., Wolfe 3rd, L., Woolford, A.J., Wu, Z., Yan, H. & Kerns, J.K. (2019). Structure-Activity and Structure-Conformation Relationships of Aryl Propionic Acid Inhibitors of the Kelch-like ECH-Associated Protein 1/Nuclear Factor Erythroid 2-Related Factor 2 (KEAP1/NRF2) Protein-Protein Interaction, *J. Med. Chem*. 62(9), 4683–4702. DOI: 10.1021/acs.jmedchem.9b00279.

27. Limeng, S., Yun B., Ying S., Libo W., Liyao A. & Qinying, Y. (2019). Nrf2 mediates the protective effect of edaravone after chlorpyrifos-induced nervous system toxicity, *Environ. Toxicol*. 34(5), 626–633. DOI: 10.1002/tox.22728.

28. Daina, A., Michielin, O. & Zoete, V. (2017). Swiss ADME: a free web tool to evaluate pharmacokinetics, druglikeness and medicinal chemistry friendliness of small molecules. *Sci. Rep*. 7, 42717. DOI: 10.1038/srep42717.